Available online at www.sciencedirect.com
ScienceDirect
Journal of Hazardous Materials 149 (2007) 199–207
Journal of Hazardous Materials
www.elsevier.com/locate/jhazmat

Effect of alumina on photocatalytic activity of iron oxides for bisphenol A degradation

F.B. Li [a,b], X.Z. Li [a,*], C.S. Liu [b], T.X. Liu [b]

[a] *Department of Civil and Structural Engineering, The Hong Kong Polytechnic University, Kowloon, Hong Kong, China*
[b] *Guangdong Key Laboratory of Agricultural Environment Pollution Integrated Control, Guangdong Institute of Eco-Environment and Soil Science, Guangzhou 510650, China*

Received 16 November 2006; received in revised form 16 March 2007; accepted 16 March 2007
Available online 27 March 2007

Abstract

To study the photodegradation of organic pollutants at the interface of minerals and water in natural environment, three series of alumina-coupled iron oxides (Al_2O_3–Fe_2O_3-300, Al_2O_3–Fe_2O_3-420, and Al_2O_3–Fe_2O_3-550) with different alumina fraction were prepared and characterized by X-ray diffraction (XRD), Brunauer–Emmett–Teller (BET) and Barret–Joyner–Halender (BJH), and Fourier transform infrared spectra (FTIR). The XRD results showed that existence of alumina in iron oxides could hinder the formation of maghemite and hematite, and also the crystal transformation from maghemite to hematite during sintering. It has been confirmed that the BET surface area and micropore surface area of Al_2O_3–Fe_2O_3 catalysts increased with an increased dosage of alumina and with decreased sintering temperature. The pore size distribution also depended on the fraction of alumina. Furthermore, all Al_2O_3–Fe_2O_3 catalysts had a mixed pore structure of micropore, mesopore and macropore. FTIR results showed that FTIR peaks attributable to Fe–O vibrations of maghemite or hematite were also affected by alumina content and sintering temperature. It was confirmed that the crystal structure and crystalline, the surface area and pore size distribution of Al_2O_3–Fe_2O_3 catalysts depend strongly on the content of alumina and also sintering temperature. Bisphenol A (BPA) was selected as a model endocrine disruptor in aquatic environment. The effects of alumina on the photocatalytic activity of iron oxides for BPA degradation were investigated in aqueous suspension. The experimental results showed that the dependence of BPA degradation on the alumina content was attributable to the crystal structure, crystalline and also the properties of their surface structures. It was confirmed that the mixed crystal structure of maghemite and hematite could achieve the higher photocatalytic activity than maghemite or hematite alone.

Keywords: Alumina; Bisphenol A; Hematite; Iron oxides; Maghemite; Photodegradation

1. Introduction

Since soil and water on the earth surface suffer from contamination of organic pollutants extensively at different degrees from ppb to ppm levels, it has become important to better understand some abiotic transformations of these organic pollutants naturally occurring in the environment, such as some catalytic processes at mineral surfaces. Actually these processes may play a vital role in decontamination and mineralization of organic pollutants under a natural condition [1–3]. It is necessary to investigate the catalytic properties and activity of these minerals in such catalytic processes. Since these catalytic processes involve some complicated heterogeneous reactions between minerals and water, the interactive reactions occurring at the mineral–water interface become critical to influence the processes of decontamination in the natural environment [4–7].

Iron oxides, including oxyhydroxides, are a kind of natural minerals and geocatalysts, naturally existing in the earth's crust with great content [8]. Since these iron oxides are very reactive, a number of secondary iron oxides such as maghemite (γ-Fe_2O_3), hematite (α-Fe_2O_3), lepidocrocite (γ-FeOOH), goethite (α-FeOOH), ferrihydrite ($Fe_5HO_8{\cdot}4H_2O$), and magnetite (Fe_3O_4) were found in aqueous streams as suspended materials with a significant amount [1–3]. Hence, the iron oxides in aquatic ecosystems play a vital role in a variety of chemical and

* Corresponding author. Tel.: +852 2766 6016; fax: +852 2334 6389.
E-mail addresses: cefbli@soil.gd.cn (F.B. Li), cexzli@polyu.edu.hk (X.Z. Li).

0304-3894/$ – see front matter © 2007 Elsevier B.V. All rights reserved.
doi:10.1016/j.jhazmat.2007.03.069

biological processes relevant to the transformation of organic compounds.

γ-Fe_2O_3 and α-Fe_2O_3 are two common iron oxides to show semiconductor properties with a narrow band gap of 2.0–2.3 eV and might be photoactive under solar irradiation as photocatalysts or photosensitizers [9,10] as described by the following equations:

$$Fe_2O_3 + h\nu \rightarrow e^- + h^+ \quad (1)$$

$$O_2 + e^- \rightarrow O_2^{\bullet -} \quad (2)$$

$$O_2^{\bullet -} + 2H^+ \rightarrow 2^{\bullet}OH \quad (3)$$

It has been widely recognized that the iron oxide surface may play an important role as catalysts for photochemical transformations [11–16]. Cunningham et al. [17] obtained the evidence of the photocatalytic formation of $^{\bullet}OH$ radical in aqueous suspensions of α-FeOOH under visible illumination, even though the photochemical transformation rate for organic degradation was found to be at a lower level. On the other hand, different Fe_2O_3 as natural minerals exist in our natural environment usually not alone and they very often coexist with silicate and alumina in soil. The fraction of silicate and alumina in clay varies in a board range from very low up to 75% [1–3]. However, these silicate and alumina are normally not photoactive under light irradiation at a wavelength of longer than 200 nm owing to their wide band gaps. Meanwhile, alumina-supported iron oxides were also investigated extensively as a kind of industrial catalysts [18–20].

In this study, three series of alumina-iron oxide (Al_2O_3–Fe_2O_3) samples with different fraction of alumina up to 70% were prepared as photocatalysts and their photocatalytic activity was evaluated in the degradation of bisphenol A (BPA) as a model endocrine disrupting chemical (EDC) in aqueous solution under UV-A illumination to study the effects of alumina on the photocatalytic activity of iron oxides, since BPA has been extensively used as a raw material of epoxy and polycarbonate resins, and also as antioxidants in softeners, fungicides, and similar products at about 1700 tonnes annually all over the world [21,22].

2. Experimental

2.1. Preparation of Fe_2O_3 and Al_2O_3–Fe_2O_3 powders

Three Fe_2O_3 powder samples were first prepared from $Fe(NO_3)_3{\cdot}9H_2O$ and glycol by a sol–gel procedure that 0.1 mol of $Fe(NO_3)_3{\cdot}9H_2O$ was dissolved into 160 ml of glycol and stirred sufficiently; then the solution was refluxed in a 250 ml flask at 65 °C for 24 h to get hydrosol; the hydrosol was dried at 100 °C for 24 h to obtain xerogel; then the xerogel was ground and sintered at 300, 420, and 550 °C for 2 h, respectively. The three product Fe_2O_3 powders were named "Fe_2O_3-300" "Fe_2O_3-420" and "Fe_2O_3-550".

Three series of Al_2O_3–Fe_2O_3 powders were then prepared from $Fe(NO_3)_3{\cdot}9H_2O$, $Al(NO_3)_3{\cdot}9H_2O$, and glycol by the similar procedure, in which 0.1 mol of mixture of $Fe(NO_3)_3{\cdot}9H_2O$ and $Al(NO_3)_3{\cdot}9H_2O$ was dissolved into 160 ml of glycol with different molar ratios of Al/(Fe + Al). The first series of Al_2O_3–Fe_2O_3 powder samples with the alumina contents of 70%, 60%, 50%, 40%, 30%, 20%, 10% and 5% were sintered at 300 °C for 2 h and named "Al_2O_3(0.7)–Fe_2O_3-300", "Al_2O_3(0.6)–Fe_2O_3-300", "Al_2O_3(0.5)–Fe_2O_3-300", "Al_2O_3(0.4)–Fe_2O_3-300", "Al_2O_3(0.3)–Fe_2O_3-300", "Al_2O_3(0.2)–Fe_2O_3-300", "Al_2O_3(0.1)–Fe_2O_3-300", and "Al_2O_3(0.05)–Fe_2O_3-300". Then other two series of Al_2O_3–Fe_2O_3-420 and Al_2O_3–Fe_2O_3-550 samples were prepared in the same way, but sintered at higher temperatures of 420 and 550 °C for 2 h, respectively and named "Al_2O_3(0.7)–Fe_2O_3-420", "Al_2O_3(0.6)–Fe_2O_3-420", "Al_2O_3(0.5)–Fe_2O_3-420", "Al_2O_3(0.4)–Fe_2O_3-420", "Al_2O_3(0.3)–Fe_2O_3-420", "Al_2O_3(0.2)–Fe_2O_3-420", "Al_2O_3(0.1)–Fe_2O_3-420", "Al_2O_3(0.05)–Fe_2O_3-420"; "Al_2O_3(0.7)–Fe_2O_3-550", "Al_2O_3(0.6)–Fe_2O_3-550", "Al_2O_3(0.5)–Fe_2O_3-550", "Al_2O_3(0.4)–Fe_2O_3-550", "Al_2O_3(0.3)–Fe_2O_3-550", "Al_2O_3(0.2)–Fe_2O_3-550", "Al_2O_3(0.1)–Fe_2O_3-550", and "Al_2O_3(0.05)–Fe_2O_3-550", respectively. Alumina content is defined as the molar ratios of Al/(Fe + Al) from aluminum salt and ferric salt in this investigation.

2.2. Characterization of Fe_2O_3 and Al_2O_3–Fe_2O_3 samples

To determine the crystal phase composition of the prepared catalysts, X-ray diffraction (XRD) measurement was carried out at room temperature using a Rigaku D/MAX-IIIA diffractometer with Cu Kα radiation (λ = 0.15418 nm). The accelerating voltage of 35 kV and the emission current of 30 mA were used. The BET surface area, micropore surface area, and total pore volume of all samples were measured by the Brunauer–Emmett–Teller (BET) method, in which the N_2 adsorption at 77 K using a Carlo Erba Sorptometer was applied. The pore-size distribution of the catalysts was determined by the Barrett–Joyner–Halenda (BJH) method [23,24]. Fourier transform infrared spectra of the catalysts were also recorded with a FT-IR spectrometer (Bruker Optics EQUINOX 55) at room temperature [25].

2.3. Experimental setup and procedures

A Pyrex cylindrical photoreactor with an effective volume of 250 ml was used to conduct photocatalytic degradation experiments, which is surrounded by a Pyrex circulating water jacket to control the temperature at 25 ± 2 °C during the reaction. An 8-W UV lamp (Luzchem Research, Inc.) with a main emission at 365 nm is positioned at the centre of the cylindrical vessel and used for photoreaction under UV-A irradiation at the light intensity of 1.2 mW cm^{-2}. The photoreactor is covered with aluminium foil to keep it away from any indoor light interference.

BPA chemical (2,2-bis(4-hydroxyphenyl)propane) with analytical grade was purchased from Aldrich and used without further purification to prepare aqueous BPA solution. The reaction suspension was prepared by adding 0.25 g of catalyst powder into 250 ml of aqueous BPA solution. Prior to the photoreaction, the suspension was magnetically stirred in the dark for 30 min to establish an adsorption/desorption equilibrium between solution and solid catalyst first and then was irradi-

ated by the UV lamp with constant aeration. At the given time intervals, the analytical samples were taken from the suspension with immediate centrifugation for 20 min and then filtered with a 0.45 μm Millipore filter to remove the particles. All samples were then stored in the dark prior to analyses.

2.4. Analytical methods

BPA in aqueous samples were analyzed by high pressure liquid chromatography (Finnigan LCQ DUO), which consists of a gradient pump (Spectra System P4000), an autosampler (Spectra System Tem AS3000) with a 20 μl injection loop, and a photodiode array UV detector (Spectra SYSTEM UV6000LP). A Pinnacle II column (C18, 5 μm, 250 mm × 4.6 mm ID) was used for BPA separation with a mobile phase (70% HCN: 30% water) at a flow rate of 0.8 ml min^{-1}. The BPA concentration was determined by the UV detector at 278 nm. Total dissolved Fe ions (TD-Fe) was analyzed by atomic absorption spectrometry (AAS).

3. Results and discussion

3.1. The effect of alumina on the crystal structure of catalysts

Three series of Al_2O_3–Fe_2O_3 samples including Fe_2O_3 samples were examined by XRD and their XRD patterns are shown in Fig. 1. For the Al_2O_3–Fe_2O_3-300 series, while Fe_2O_3-300 sample showed five peaks (2 2 0, 3 1 1, 4 2 1, 5 1 1, and 4 4 0) attributable to maghemite and three peaks (0 1 2, 1 0 4, and 1 1 3) attributable to hematite, based on the Joint Committee on Powder Diffraction Standards, indicating a mixed crystal structure of maghemite and hematite, the Al_2O_3–Fe_2O_3-300 samples showed a relatively weaker crystal structure of maghemite with an increased fraction of alumina. Furthermore, it can be seen that while Al_2O_3(0.05)–Fe_2O_3-300, Al_2O_3(0.1)–Fe_2O_3-300 and Al_2O_3(0.2)–Fe_2O_3-300 showed five strong peaks of maghemite, Al_2O_3(0.3)–Fe_2O_3-300, Al_2O_3(0.4)–Fe_2O_3-300, and Al_2O_3(0.5)–Fe_2O_3-300 showed only four peaks (2 2 0, 3 1 1, 5 1 1 and 4 4 0) with much lower intensity, and Al_2O_3(0.6)–Fe_2O_3-300 and Al_2O_3(0.7)–Fe_2O_3-300 showed almost an amorphous structure. These results indicate that introducing alumina could delay the crystallization of iron oxides during the sintering treatment.

For the Al_2O_3–Fe_2O_3-420 series, while the Fe_2O_3-420 sample showed a crystal structure of almost hematite with eight peaks (0 1 2, 1 0 4, 1 1 0, 1 1 3, 0 2 4, 1 1 6, 2 1 4, and 3 0 0), the Al_2O_3(0.05)–Fe_2O_3-420 and Al_2O_3(0.1)–Fe_2O_3-420 samples showed a mixed structure of maghemite and hematite with both types of peaks (0 1 2, 2 2 0, 1 0 4, 3 1 1, 1 1 3, 0 2 4, 1 1 6, 5 1 1, and 4 4 0), the Al_2O_3(0.2)–Fe_2O_3-420, Al_2O_3(0.3)–Fe_2O_3-420, Al_2O_3(0.4)–Fe_2O_3-420, Al_2O_3(0.5)–Fe_2O_3-420 and Al_2O_3(0.6)–Fe_2O_3-420 samples showed four peaks of maghemite (2 2 0, 3 1 1, 5 1 1 and 4 4 0), and the Al_2O_3(0.7)–Fe_2O_3-420 sample showed almost an amorphous structure. These results indicate that introducing alumina does not only delay the crystallization, but also could hinder the crystal transformation of iron oxides from maghemite to hematite during sintering treatment.

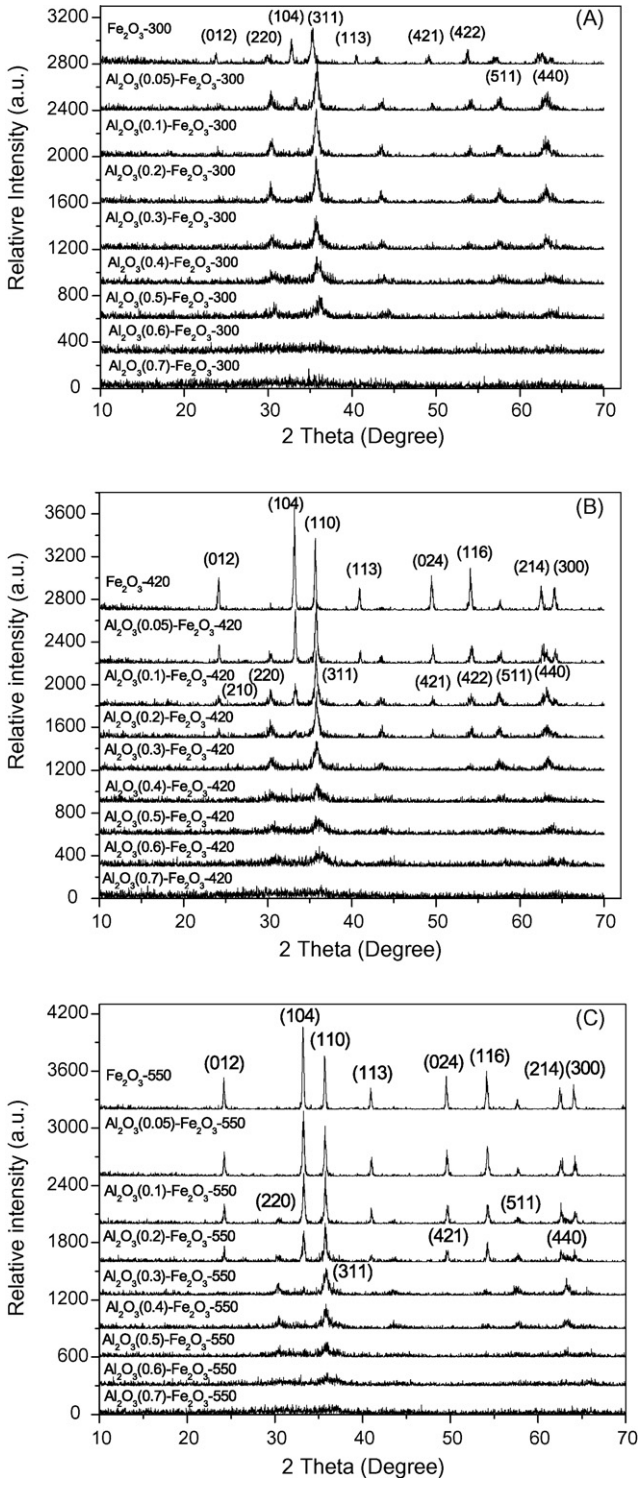

Fig. 1. The XRD patterns of different iron oxides sintered at 300 °C (A), 420 °C (B) and 550 °C (C).

For the Al_2O_3–Fe_2O_3-550 series, while the Fe_2O_3-550 and Al_2O_3(0.05)–Fe_2O_3-550 samples showed a typical structure of hematite with eight peaks (0 1 2, 1 0 4, 1 1 0, 1 1 3, 0 2 4, 1 1 6, 2 1 4, and 3 0 0), the Al_2O_3(0.1)–Fe_2O_3-550 and Al_2O_3(0.2)–Fe_2O_3-550 samples showed a mixed

structure of maghemite and hematite with the nine peaks (012, 104, 113, 024, 116, 214, 300, 311 and 220), and the Al_2O_3(0.3)–Fe_2O_3-550, Al_2O_3(0.4)–Fe_2O_3-550, Al_2O_3(0.5)–Fe_2O_3-550, and Al_2O_3(0.6)–Fe_2O_3-550 samples showed almost a crystal structure of maghemite only. In the meantime, the Al_2O_3(0.7)–Fe_2O_3-550 sample remained its amorphous structure. From the above results, it is clear that the increase of sintering temperature will enhance crystal transformation of iron oxides from maghemite to hematite significantly. Furthermore, it can be indicated that the existence of alumina would delay the crystallization of iron oxides and also might hinder the crystal transformation of iron oxides from maghemite to hematite as well.

The three series of catalysts with different crystal structures are summarized in Table 1. Therefore, no any peak presented was attributable to alumina or the solid solutions of Al_2O_3 and Fe_2O_3. That implies that alumina should be amorphous structure. In fact, crystallized alumina such as γ-Al_2O_3 might present under thermal treatment at 800 °C and α-Al_2O_3 might present under thermal treatment at 1000 °C [19,20].

3.2. The effect of alumina on the BET surface area and pore size distribution of catalysts

The BET surface area and the pore structure of different catalysts were determined from nitrogen isothermal analyses. Their nitrogen adsorption–desorption isothermal curves are shown in Fig. 2 (A for Al_2O_3–Fe_2O_3-300; B for Al_2O_3–Fe_2O_3-420 and C for Al_2O_3–Fe_2O_3-550). It can be seen that the adsorbed nitrogen volume decreased with increased temperature significantly and their isotherms had a combined shape of type I and type IV with two distinct regions: at a low relative pressure, isotherms exhibited high adsorption, indicating that the catalyts contained micropores (type I) [23,24,26,27]. In addition, the curves also exhibited hysteresis loops at a high relative pressure, indicating the presence of micropores and also mesopores. The distribution of these hysteresis loops depended on the content of alumina. The shape of the hysteresis loops are of type H3.

The results of pore size distribution for different catalysts are shown in Fig. 3 (A for Al_2O_3–Fe_2O_3-300, B for Al_2O_3–Fe_2O_3-420, and C for Al_2O_3–Fe_2O_3-550). It can be seen that the pore size distribution strongly depended on the alumina content and also sintering temperature. Fe_2O_3-300 showed a mixture pore size of mesopores and macropores with a significant peak at 18.36 nm, while Fe_2O_3-420 showed a mixture pore size of mesopores and macropores with the peak at 30.17 nm. For three series, all catalysts except for Fe_2O_3-300 and Fe_2O_3-420 showed a mixture pore size of micropore, mesopores and macropores, while pore sizes distributed from 1 up to 160 nm, and pore volumes decreased significantly with the increase of pore sizes for other catalysts.

The analytical data for the BET surface area, micropore surface area, and micropore volume of different catalysts are also summarized in Table 1. It is clear that both the BET surface area and micropore surface area of all catalysts are dependent on sintering temperature and also alumina content and increased with increased amount of alumina content significantly, but decreased

Table 1
The crystal structure, BET surface area, micropore surface area and micropore volume of iron oxides

Iron oxides	Al_2O_3(0.7)–Fe_2O_3-300	Al_2O_3(0.5)–Fe_2O_3-300	Al_2O_3(0.3)–Fe_2O_3-300	Al_2O_3(0.2)–Fe_2O_3-300	Al_2O_3(0.1)–Fe_2O_3-300	Fe_2O_3-300
Crystal structure	Amorphous	γ-Fe_2O_3	γ-Fe_2O_3	γ-Fe_2O_3	γ-Fe_2O_3	γ + α-Fe_2O_3
BET surface area ($m^2\,g^{-1}$)	115.32	88.46	87.25	81.36	63.37	26.93
Micropore surface area ($m^2\,g^{-1}$)	28.57	7.45	4.56	3.65	2.38	1.27
Micropore volume ($cm^3\,g^{-1}$)	0.012	0.0033	0.00016	0.0029	0.0012	0.0003
Iron oxides	Al_2O_3(0.7)–Fe_2O_3-420	Al_2O_3(0.5)–Fe_2O_3-420	Al_2O_3(0.3)–Fe_2O_3-420	Al_2O_3(0.2)–Fe_2O_3-420	Al_2O_3(0.1)–Fe_2O_3-420	Fe_2O_3-420
Crystal structure	Amorphous	γ-Fe_2O_3	γ-Fe_2O_3	γ-Fe_2O_3	γ + α-Fe_2O_3	α-Fe_2O_3
BET surface area ($m^2\,g^{-1}$)	98.96	68.65	61.43	55.69	40.737	12.92
Micropore surface area ($m^2\,g^{-1}$)	25.23	4.107	2.924	2.57	1.351	0.15
Micropore volume ($m^3\,g^{-1}$)	0.010	0.00066	0.00057	0.00071	0.0012	0.0000
Iron oxides	Al_2O_3(0.7)–Fe_2O_3-550	Al_2O_3(0.5)–Fe_2O_3-550	Al_2O_3(0.3)–Fe_2O_3-550	Al_2O_3(0.2)–Fe_2O_3-550	Al_2O_3(0.1)–Fe_2O_3-550	Fe_2O_3-550
Crystal structure	Amorphous	γ-Fe_2O_3	γ-Fe_2O_3	γ + α-Fe_2O_3	γ + α-Fe_2O_3	α-Fe_2O_3
BET surface area ($m^2\,g^{-1}$)	72.17	67.66	60.63	41.87	27.94	7.82
Micropore surface area ($m^2\,g^{-1}$)	5.0455	2.3066	1.0396	0.7295	0	0
Micropore volume ($m^3\,g^{-1}$)	0.00223	0.00117	0.00059	0.00043	0	0

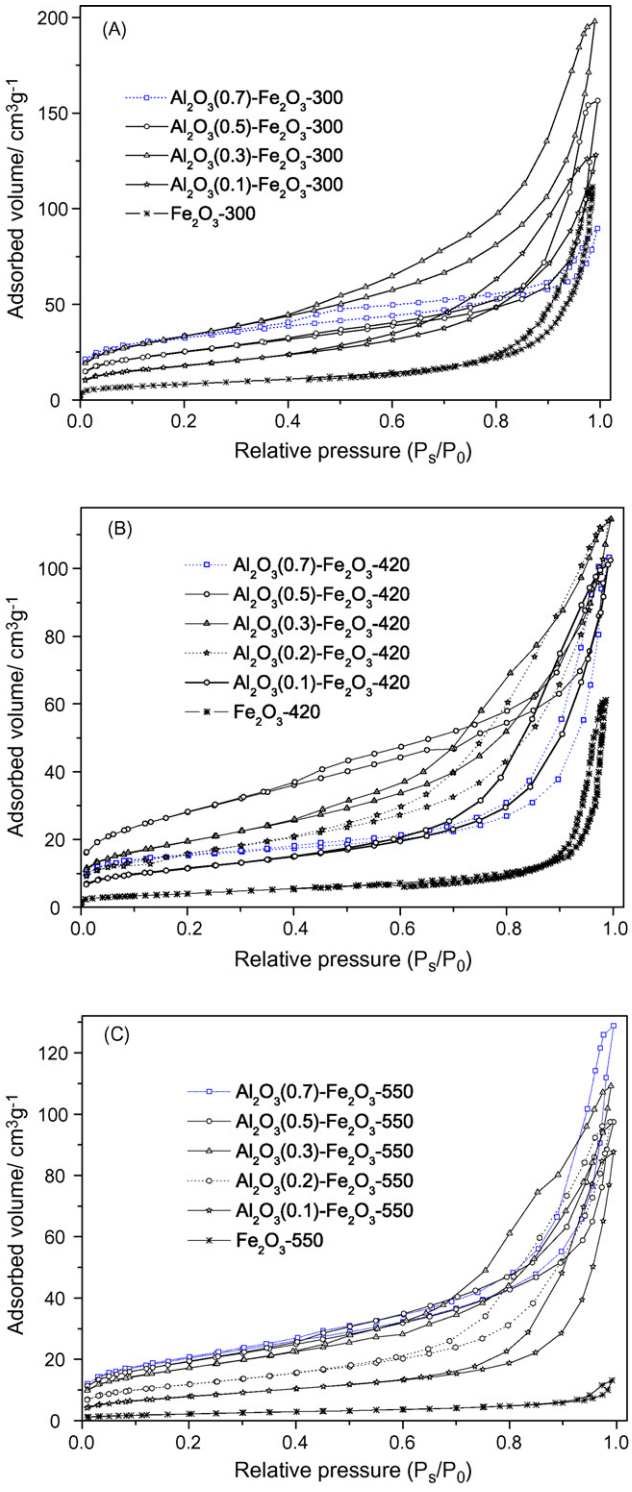

Fig. 2. The nitrogen adsorption–desorption isothermal curves of Fe_2O_3–Al_2O_3 powders sintered at 300 °C (A), 420 °C (B) and 550 °C (C).

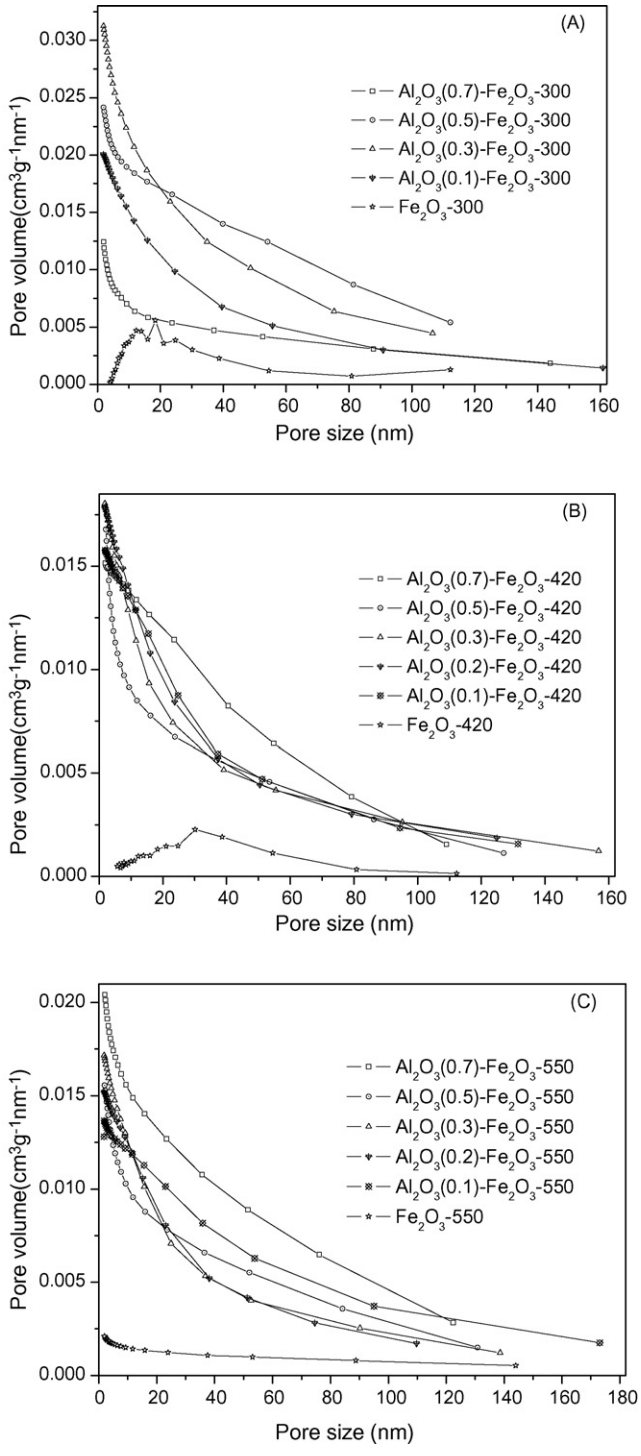

Fig. 3. The pore size distribution of Fe_2O_3–Al_2O_3 powders sintered at 300 °C (A), 420 °C (B) and 550 °C (C).

with increased sintering temperature at the same content of alumina. These results revealed that the $Al_{0.7}$–Fe_2O_3-300 catalyst had the largest BET surface area of 115.32 $m^2\,g^{-1}$ and also the highest micropore volume of 28.57 $m^2\,g^{-1}$, while the Fe_2O_3-550 catalyst had the lowest BET surface area of 7.82 $m^2\,g^{-1}$.

3.3. The effect of alumina on the chemical state of catalysts

The FTIR transmittance spectra from 4000 to 400 cm^{-1} are shown in Fig. 4 (A for Al_2O_3–Fe_2O_3-300, B for Al_2O_3–Fe_2O_3-420, and C for Al_2O_3–Fe_2O_3-550) to investigate the effect of alumina on the chemical state of catalysts. For all catalysts, the broad peaks in the range of 3350–3450 cm^{-1} and the narrow peak at about 1620 cm^{-1} are attributable to the O–H stretch-

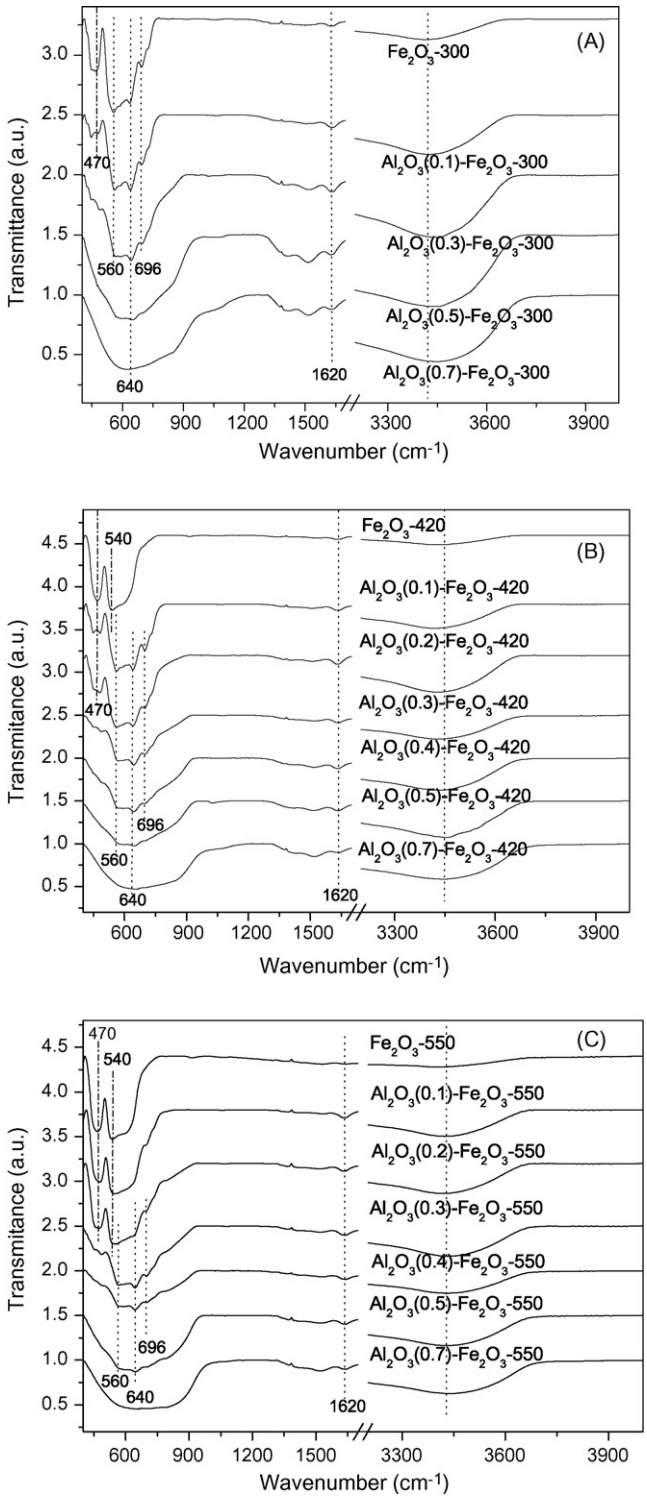

Fig. 4. The FTIR transmittance spectra of Fe_2O_3–Al_2O_3 powders sintered at 300 °C (A), 420 °C (B) and 550 °C (C).

ing vibration of water and an OH group on the surface of iron oxides. The peaks at 470 and 540 cm^{-1} should be attributable to the Fe–O vibration of hematite for Fe_2O_3-300, Fe_2O_3-420, Al_2O_3(0.1)–Fe_2O_3-420, Fe_2O_3-550, Al_2O_3(0.1)–Fe_2O_3-550, and Al_2O_3(0.2)–Fe_2O_3-550, while the peaks at 560, 640, and 696 cm^{-1} should be attributable to the Fe–O vibration of maghemite, as labelled in Fig. 4 [8,18–20].

3.4. The effect of alumina on the photocatalytic degradation of BPA

Under UV-A illumination, iron oxides can be excited to generate holes and electrons, and the excited electrons are further transferred to oxygen to form hydroxyl radicals as described by Eqs. (1)–(3). BPA in the reaction solution is then attacked by the hydroxyl radicals to be degraded. To investigate the effect of alumina on the photocatalytic activity of iron oxides in BPA degradation, three sets of experiments were carried out in aqueous BPA suspension with an initial concentration of 0.044 mM and 1 $g\,l^{-1}$ of catalyst under UV-A illumination and each experiment lasted for 150 min. The experimental results are shown in Fig. 5. By assuming that the photocatalytic degradation of BPA in aqueous suspension follows the first-order kinetics, the first-order kinetic constants, k, can be calculated by fitting the experimental data and are compared in Table 2.

For the Al_2O_3–Fe_2O_3-300 series, it can be seen that while the Fe_2O_3-300 catalyst had the highest k value, the Al_2O_3–Fe_2O_3-300 catalysts had lower k values that are decreased with increased fraction of alumina. Since the Al_2O_3–Fe_2O_3-300 catalysts with higher fraction of alumina were more amorphous, it implies that the higher crystalline of maghemite might lead to the higher photocatalytic activity. For the Al_2O_3–Fe_2O_3-420 series and Al_2O_3–Fe_2O_3-550 series, both the Al_2O_3(0.1)–Fe_2O_3-420 and Al_2O_3(0.1)–Fe_2O_3-550 catalysts had the highest k values in their temperature series, respectively, which indicate that the iron oxides with 10% alumina had the highest activity for BPA degradation under UV-A illumination. Comparing three series of catalysts sintered at different temperatures, it is significant that the Al_2O_3–Fe_2O_3-420 series had higher k values than the Al_2O_3–Fe_2O_3-300 and Al_2O_3–Fe_2O_3-550 series.

From the above experimental results, it may be summarized that the photocatalytic activity of iron oxides should depend on a number of their characteristics such as crystalline, crystal structure, surface structure properties, surface area and so on. Among them, the crystalline and crystal structure might play more critical roles than the surface structure properties in BPA degradation under these experimental conditions. For the catalysts sintered at a same temperature, the effect of alumina on photocatalytic activity might result from their different crystalline and crystal structure. The experiments in this study demonstrated that the catalysts containing a mixture of maghemite and hematite had the higher activity than those containing either maghemite or hematite alone. Actually two band gaps of maghemite (2.03 eV) and hematite (2.02 eV) are very close, but they have different positions. While hematite has a conduction band level at −0.62 V and a valence band level at +1.40 V, maghemite has the two band levels at −0.08 and +1.94 V, respectively [10]. In their mixture, the excited electrons at the conduction band of hematite would transfer to the conduction band of maghemite easily, which results in an effective electron separation and transformation within the iron oxides. Furthermore, the maghemite catalysts with a higher crystalline degree had the higher photocatalytic activity.

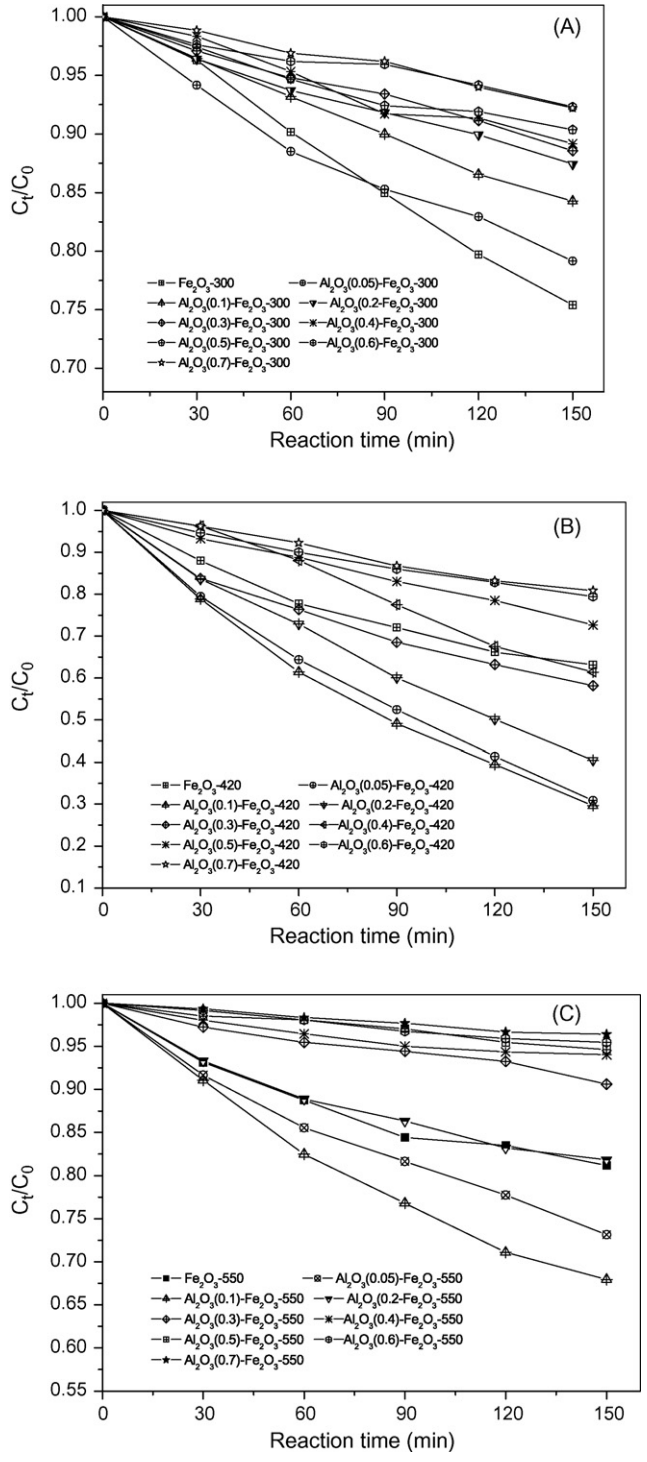

Fig. 5. The photocatalytic degradation of BPA under UV-A illumination using different iron oxides sintered at 300 °C (A), 420 °C (B) and 550 °C (C).

It is well known that many iron oxides in an acidic solution can be dissolved by light irradiation to release Fe^{3+} ion as shown below:

$$Fe_2O_3 + H^+ + h\nu \rightarrow Fe^{3+} + H_2O \quad (4)$$

$$Fe_2(OH)_2{}^{4+} + h\nu \rightarrow Fe^{2+} + {}^{\bullet}OH \quad (5)$$

Table 2
The first-order-kinetic constants k (min^{-1}) for BPA degradation under UV-A illumination using different catalysts

Catalysts	k	R^2	Catalysts	k	R^2	Catalysts	k	R^2
Fe_2O_3-300	0.0018	0.9928	Fe_2O_3-420	0.0034	0.9612	Fe_2O_3-550	0.0016	0.9689
$Al_2O_3(0.05)$–Fe_2O_3-300	0.0016	0.9710	$Al_2O_3(0.05)$–Fe_2O_3-420	0.0075	0.9959	$Al_2O_3(0.05)$–Fe_2O_3-550	0.0022	0.9773
$Al_2O_3(0.1)$–Fe_2O_3-300	0.0012	0.9982	$Al_2O_3(0.1)$–Fe_2O_3-420	0.0080	0.9988	$Al_2O_3(0.1)$–Fe_2O_3-550	0.0028	0.9882
$Al_2O_3(0.2)$–Fe_2O_3-300	0.0009	0.9817	$Al_2O_3(0.2)$–Fe_2O_3-420	0.0058	0.9958	$Al_2O_3(0.2)$–Fe_2O_3-550	0.0015	0.9655
$Al_2O_3(0.3)$–Fe_2O_3-300	0.0008	0.9905	$Al_2O_3(0.3)$–Fe_2O_3-420	0.0039	0.9612	$Al_2O_3(0.3)$–Fe_2O_3-550	0.0006	0.9662
$Al_2O_3(0.4)$–Fe_2O_3-300	0.0008	0.9690	$Al_2O_3(0.4)$–Fe_2O_3-420	0.0031	0.9585	$Al_2O_3(0.4)$–Fe_2O_3-550	0.0005	0.9625
$Al_2O_3(0.5)$–Fe_2O_3-300	0.0007	0.9480	$Al_2O_3(0.5)$–Fe_2O_3-420	0.0021	0.9967	$Al_2O_3(0.5)$–Fe_2O_3-550	0.0004	0.9832
$Al_2O_3(0.6)$–Fe_2O_3-300	0.0005	0.9569	$Al_2O_3(0.6)$–Fe_2O_3-420	0.0016	0.9928	$Al_2O_3(0.6)$–Fe_2O_3-550	0.0003	0.9848
$Al_2O_3(0.7)$–Fe_2O_3-300	0.0005	0.9818	$Al_2O_3(0.7)$–Fe_2O_3-420	0.0015	0.9916	$Al_2O_3(0.7)$–Fe_2O_3-550	0.0003	0.9858

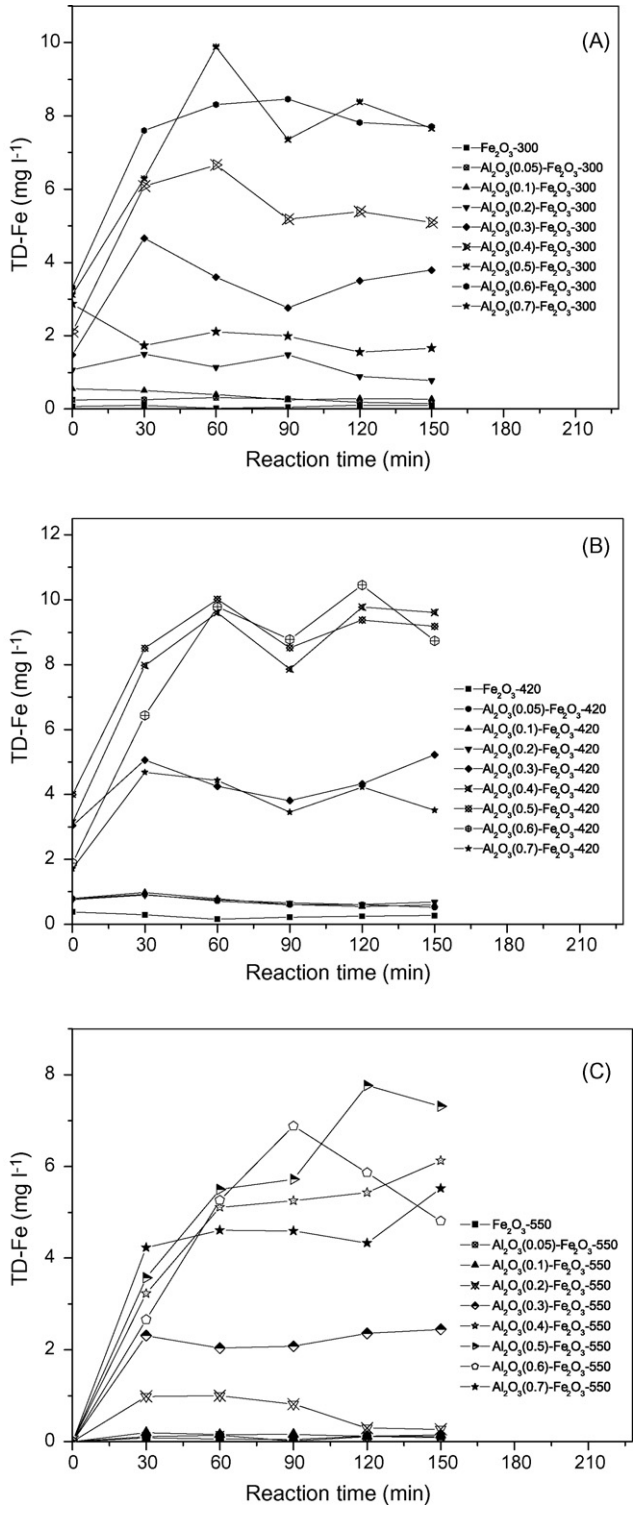

Fig. 6. The photo-dissolution of different iron oxides sintered at 300 °C (A), 420 °C (B) and 550 °C (C) under UV-A illumination vs. reaction time.

In this study, the concentration of total dissolved Fe (TD-Fe) during photoreaction was determined by AAS and the results are shown in Fig. 6. The experiments demonstrated that most iron oxides released Fe^{3+} into the aqueous suspension during the reaction and the TD-Fe concentrations were quickly increased after a short reaction time and then gradually reached their maximum levels and maintained until the end of experiments at 150 min. It can be seen that the iron oxides with 40–60% alumina released more Fe^{3+} than others for three series of catalysts sintered at different temperatures. In fact, such a photo-dissolution of iron oxides depends on the crystalline and also crystal structure of iron oxides. In general, maghemite is more easily photo-dissolved than hematite, and iron oxides with higher crystalline are more difficult to be photo-dissolved than those with lower crystalline. On the other hand, the degree of iron dissolution also depends on pH. The dominant specie in the absence of organic ligand is $Fe_2(OH)_2^{4+}$ in weak acidic solution, which could be further photoreduced to form hydroxyl radical and Fe^{2+} as shown by reaction (5). However, the quantum yield for the formation of hydroxyl radical is only 0.017 at 360 nm [28–30], the BPA degradation under UV-A illumination at 365 nm was affected by the dissolution of iron oxides and the formation of dissolved ferric ion at a minor degree for iron oxides with a higher crystalline and activity, and at a significant degree for iron oxides with a lower crystalline under this experimental condition. The excitation of dissolved ferric ion under UV-A illumination might play a sole role in BPA degradation for catalysts with amorphous structure.

4. Conclusions

It could be confirmed that the crystal structure and crystalline, the surface area and pore size distribution of Al_2O_3–Fe_2O_3 catalysts depend strongly on the content of alumina and also sintering temperature. The existence of alumina could hinder the crystallization of iron oxides and also crystal transformation from maghemite to hematite during sintering. The BET surface area and micropore surface area increased significantly with an increased content of alumina, but decreased with an increased sintering temperature. The dependence of BPA degradation on the alumina content was attributable to the crystal structure, crystalline and also the properties of surface structures of Al_2O_3–Fe_2O_3 catalysts.

Acknowledgements

The authors would thank the Hong Kong Government Research Grant Committee for a financial support to this work (RGC No. PolyU 5170/04E), and also thank the China National Natural Science Foundation (Project No. 20377011) and the Guangdong Natural Science Foundation (Project No. 036533).

References

[1] M.A.A. Schoonen, Y. Xu, D.R. Strongin, An introduction to geocatalysis, Geochem. Exploration 62 (1998) 201–215.
[2] F.E. Rhoton, J.M. Bigham, D.L. Lindbo, Properties of iron oxides in streams draining the Loess Uplands of Mississippi, Appl. Geochem. 17 (2002) 409–419.
[3] C. Swearingen, S. Macha, A. Fitch, Leashed ferrocenes at clay surfaces: potential applications for environmental catalysis, J Mol. Catal. A: Chem. 199 (2003) 149–160.
[4] P. Behra, L. Sigg, Evidence for redox cycling of iron in atmospheric water droplets, Nature 344 (1990) 419–421.

[5] T.J. Grundl, D.L. Sparks, Kinetics and mechanisms of reactions at the mineral–water interface: an overview, in: D.L. Sparks, T.J. Grundl (Eds.), Mineral–Water Interfacial Reactions: Kinetics and Mechamisms, American Chemical Society, Washington, DC, 1998, pp. 2–13.
[6] X.Z. Li, C.M. Fan, Y.P. Sun, Enhancement of photocatalytic oxidation of humic acid in TiO_2 suspensions by increasing cation strength, Chemosphere 48 (2002) 453–460.
[7] F. Keppler, R. Eiden, V. Niedan, J. Pracht, H.F. Scholer, Halocarbons produced by natural oxidation processes during degradation of organic matter, Nature 403 (2000) 298–301.
[8] R.M. Cornell, U. Schwertmann, The Iron Oxides: Structure, Properties, Reactions, Occurrences and Uses, Wiley-VCH, New York, 2003.
[9] B.C. Faust, M.R. Hoffmann, D.W. Bahnemann, Photocatalytic oxidation of sulfur-dioxide in aqueous suspensions of alpha-Fe_2O_3, J. Phys. Chem. 93 (1989) 6371–6381.
[10] J.K. Leland, A.J. Bard, Photochemistry of colloidal semiconducting iron-oxide polymorphs, J. Phys. Chem. 91 (1987) 5076–5083.
[11] R. Andreozzi, V. Caprio, R. Marotta, Iron(III) (hydr)oxide-mediated photooxidation of 2-aminophenol in aqueous solution: a kinetic study, Water Res. 37 (2003) 3682–3688.
[12] B.C. Faust, J.M. Allen, Aqueous-phase photochemical formation of hydroxyl radical in authentic cloudwaters and fogwaters, Environ. Sci. Technol. 27 (1993) 1221–1224.
[13] H.B. Fu, X. Quan, Z.Y. Liu, S. Chen, Photoinduced transformation of gamma-HCH in the presence of dissolved organic matter and enhanced photoreactive activity of humate-coated alpha-Fe_2O_3, Langmuir 20 (2004) 4867–4873.
[14] C. Kormann, D.W. Bahnemann, M.R. Hoffmann, Environmental photochemistry is iron-oxide (hematite) an active photocatalyst—a comparative-study – alpha-Fe_2O_3, ZNO, TiO_2, J. Photochem. Photobio. A: Chem. 48 (1989) 161–169.
[15] B. Pal, M.J. Sharon, Photocatalytic degradation of salicylic acid by colloidal Fe_2O_3 particles, Chem. Technol. Biotechnol. 73 (1998) 269–273.
[16] C.L. Hsueh, Y.H. Huang, C.Y. Chen, Novel activated alumina-supported iron oxide-composite as a heterogeneous catalyst for photooxidative degradation of reactive black 5, J. Hazard. Mater. B 129 (2006) 228–233.
[17] K.M. Cunningham, M.C. Goldberg, E.R. Weiner, Mechanisms for aqueous photolysis of adsorbed benzoate oxalate, and succinate on iron oxyhydroxide (goethite) surfaces, Environ. Sci. Technol. 22 (1988) 1090–1097.
[18] M.A. Karakassides, D. Gournis, A.B. Bourlinos, P.N. Trikalitis, T. Bakas, Magnetic Fe_2O_3–Al_2O_3 composites prepared by a modified wet impregnation method, J. Mater. Chem. 13 (2003) 871–876.
[19] E.A. El-Sharkawy, S.A. El-Hakam, S.E. Samra, Effect of thermal treatment on the various properties of iron(III)–aluminum(III) coprecipitated hydroxide system, Mater. Lett. 42 (2000) 331–338.
[20] W.M. Shaheen, K.S. Hong, Thermal characterization and physicochemical properties of Fe_2O_3–Mn_2O_3/Al_2O_3 system, Thermochim. Acta 381 (2002) 153–164.
[21] I.T. Cousins, C.A. Staples, G.M. Klecka, D. Mackay, A multimedia assessment of the environmental fate of bisphenol A, Hum. Ecol. Risk Assess. 8 (2002) 1107–1135.
[22] N. Watanabe, S. Horikoshi, H. Kawabe, Y. Sugie, J.C. Zhao, H. Hidaka, Photodegradation mechanism for bisphenol A at the TiO_2/H_2O interfaces, Chemosphere 52 (2003) 851–859.
[23] J.G. Yu, J.C. Yu, M.K.P. Leung, W.K. Ho, B. Cheng, X.J. Zhao, J.C. Zhao, Effects of acidic and basic hydrolysis catalysts on the photocatalytic activity and microstructures of bimodal mesoporous titania, J. Catal. 217 (2003) 69–78.
[24] S.L. Gregg, K.S.W. Sing, Adsorption, Surface Area and Porosity, Academic Press, London, 1982.
[25] H.D. Ruan, R.L. Frost, J.T. Kloprogge, L. Duong, Infrared spectroscopy of goethite dehydroxylation. III. FT-IR microscopy of in situ study of the thermal transformation of goethite to hematite, Spectrochim. Acta A 58 (2002) 967–981.
[26] J. Lei, C.S. Liu, F.B. Li, X.M. Li, S.G. Zhou, T.X. Liu, M.H. Gu, Q.T. Wu, Photodegradation of orange I in the heterogeneous iron oxide-oxalate complex system under UVA irradiation, J. Hazard. Mater. 137 (2006) 1016–1024.
[27] M.H. Zhou, J.G. Yu, B. Cheng, Effects of Fe-doping on the photocatalytic activity of mesoporous TiO2 powders prepared by an ultrasonic method, J. Hazard. Mater. 138 (2006) 1838–1847.
[28] Y.G. Zuo, J. Holgné, Formation of hydrogen-peroxide and depletion of oxalic-acid in atmospheric water by photolysis of iron(III) oxalato complexes, Environ. Sci. Technol. 26 (1992) 1014–1022.
[29] M.E. Balmer, B. Sulzberger, Atrazine degradation in irradiated iron oxalate systems: effects of pH and oxalate, Environ. Sci. Technol. 33 (1999) 2418–2424.
[30] P.L. Huston, J.J. Pignatello, Reduction of perchloroalkanes by ferrioxalate-generated carboxylate radical preceding mineralization by the photo-fenton reaction, Environ. Sci. Technol. 30 (1996) 3457–3463.